

# Probing the phases in the MSSM via $e^+e^- \rightarrow hA$

D. A. Demir\*

*Middle East Technical University, Department of Physics, 06531, Ankara, Turkey*

(November 9, 2018)

## Abstract

In the presence of the supersymmetric CP phases,  $e^+e^- \rightarrow Z^* \rightarrow hA$  scattering is analyzed, with special emphasis on  $Z^*hA$  vertex, taking into account radiative corrections due to dominant top quark and top squark loops in the Higgs sector as well as the vertex formfactors. It is found that the lightest Higgs remains essentially CP-even whereas the heavier ones mix with each other strongly. Moreover, the supersymmetric CP phases are found to create tree-level couplings between a pseudoscalar and identical sfermion mass eigenstates which, together with the radiative corrections in the Higgs sector, are found to enhance the vertex formfactors significantly.

---

\*Present Address: ICTP, Trieste, Italy.

## I. INTRODUCTION

The Minimal Supersymmetric Standard Model (MSSM) is an appealing extension of the minimal Standard Model in that it resolves the well-known gauge hierarchy problem of the latter. The MSSM Higgs sector comprises two opposite hypercharge Higgs doublets whose all quartic couplings are fixed by the gauge couplings at the tree level. In the MSSM Lagrangian, other than Yukawa couplings and the  $\mu$  parameter coming from the superpotential, there are several mass parameters in the soft supersymmetry breaking sector [1]. These parameters consist of the gaugino masses  $M_a$ , sfermion mass-squareds  $m_f^2$ , Higgs-sfermion trilinear couplings  $A_f$ , Higgs mass-squareds  $m_i^2$ , and bilinear Higgs mixing mass  $B\mu$ , all of which could, in principle, be complex. However, not all these phases are physical [2], that is, an arbitrary physical quantity depends only on certain combinations of them as dictated by the global  $U(1)$  symmetries of the MSSM Lagrangian [3]. Indeed, one can choose observable phases to be those of CKM matrix, trilinear couplings  $A_f$ , and the  $\mu$  parameter [2], and we will adopt this convention below.

For getting information about the physical implications of these phases the most convenient way is to look for the collider signatures of certain collision processes. Among others, the lepton colliders can provide a clean signature independent of the hadronic uncertainties, depending on the final state particles. In future generation of the colliders, with increasing center of mass energy of the leptons it may be possible to detect supersymmetric particles, in particular, the Higgs particles [4,5]. In this work we discuss  $e^+e^- \rightarrow hA$  scattering in the presence of explicit CP-violation in the MSSM Lagrangian through the complex  $\mu$  and  $A$  parameters. This process has been analyzed in detail in [6] at one-loop level, and radiative corrections were found to contribute  $\sim 5\%$  in regions of the parameter space where the cross section is maximized. Other than this one-loop analysis, as emphasized by Haber [7],  $hAZ$  coupling becomes vanishingly small in large  $\tan\beta - M_A$  regime. This process, compared to Bjorken process and  $W$  or  $Z$  fusion, involves two Higgs particles at the final state whose mixings and indefinite CP characteristics can affect the cross section whereby providing some information on the supersymmetry search. As will be seen below, mainly there are two distinct effects of these phases on the pair production process: (1) Mixing between the Higgs scalars due to CP-violation in the Higgs sector, and (2) loop effects of the sfermions on the  $hAZ$  vertex. Below, analytical results will be general; however, in the numerical analysis we will assume a vanishing phase for  $\mu$  in accordance with the EDM [2,8] and cosmological constraints [9] though several ways of relaxing these constraints have been suggested [10]. Recently, the supersymmetric CP phases have gotten much interest in both Higgs phenomenology [11–13] and FCNC processes [14].

## II. SUPERSYMMETRIC CP PHASES AND $E^+E^- \rightarrow HA$ SCATTERING

The supersymmetric CP phases  $\text{Arg}\{A_f\}$  and  $\text{Arg}\{\mu\}$  show up in sfermion, chargino and neutralino mass matrices so that the processes involving these particles as well as their loop effects depend on these phases explicitly [14,11–13]. In the presence of these phases there is explicit CP-violation in the Higgs sector; namely, the mass eigenstate Higgs bosons are mixtures of scalars having different CP-properties. Moreover, these phases enhance

the radiative corrections to certain quantities by introducing novel interaction vertices not found in the CP-invariant theory. In what follows we shall discuss these points in detail when analyzing the effective scalar–pseudoscalar– $Z$  boson vertex.

The loop effects of the MSSM particle spectrum on the Higgs potential could be parametrized in a simple and elegant way by applying the effective potential method [15]. Its implicit renormalization prescription corresponds to the  $\overline{DR}$  scheme. Indeed, if the theory is regularized by dimensional reduction (reducing to the usual dimensional regularization in the absence of gauge boson loops, and with the conventional algebra for Dirac matrices), in the Landau gauge, the effective potential is given by

$$V = V_0 + \frac{1}{64\pi^2} \text{Str} \mathcal{M}^4 \left( \log \frac{\mathcal{M}^2}{Q^2} - \frac{3}{2} - \Delta \right) \quad (1)$$

where  $V_0$  is the tree level MSSM potential depending on the bare parameters,  $\Delta = 2/(4 - D) - \gamma + \log 4\pi$ ,  $D$  is the dimension of spacetime,  $\gamma$  is Euler constant,  $\mathcal{M}^2$  is the field dependent mass-squared matrix of all fields, and  $Q$  is the renormalization scale. Here the renormalization scale is naturally at the weak scale and we shall take  $Q^2 \sim m_t^2$  though slightly different choices are also possible [15]. Expressing the bare parameters and fields in  $V_0$  in terms of the renormalized ones and one-loop counterterms as  $V_0 = V_{tree} + \Delta V$ , and using the *minimal* prescription  $\Delta V = \Delta \text{Str} \mathcal{M}^4 / (64\pi^2)$ , the UV divergence of (1) is cured. Here  $V_{tree}$  is the tree-level MSSM Higgs potential composed of renormalized parameters and fields only. As usual, the second order derivatives of the effective potential (1) with respect to the components of the Higgs fields, evaluated at the stationarity point, give the Higgs mass-squared matrix from which the radiatively-corrected Higgs masses and Higgs mixing matrix follow. The effective potential (1) gets the most important contributions from the top quark and top squark loops for moderate values of  $\tan \beta$  (for  $\tan \beta \sim 60$  bottom quark-squark, tau lepton-slepton contributions become important) [15]. Therefore, to a good approximation, it is sufficient to take into account only the dominant top quark and top squark loops, and neglect the contributions of other particles as justified by the analysis of [16]. Neglecting the D-term contributions, in  $(\tilde{t}_L, \tilde{t}_R)$  basis field-dependent stop mass-squared matrix is given by

$$M_{\tilde{t}} = \begin{pmatrix} M_{\tilde{t}_L}^2 + m_t^2 & h_t(A_t H_2^0 - \mu^* H_1^{0*}) \\ h_t(A_t^* H_2^{0*} - \mu H_1^0) & M_{\tilde{t}_R}^2 + m_t^2 \end{pmatrix} \quad (2)$$

where the top quark mass has the usual expression  $m_t^2 = h_t^2 |H_2^0|^2$ , and  $M_{\tilde{t}_{L,R}}^2$  are the soft mass parameters of left- and right-handed stop fields, respectively. Here  $H_{1,2}^0$  are the neutral components of the Higgs doublets, and in the true vacuum state of the MSSM,  $\langle H_2^0 \rangle = v_2/\sqrt{2}$ ,  $\langle H_1^0 \rangle = v_1/\sqrt{2}$  such that  $v_1^2 + v_2^2 = 4M_W^2/g^2$ , and  $v_2/v_1 \equiv \tan \beta$ . In this vacuum state stop mass-squared matrix (1) is diagonalized as  $U_{\tilde{t}}^\dagger M_{\tilde{t}} U_{\tilde{t}} = \text{diag}(m_{\tilde{t}_1}^2, m_{\tilde{t}_2}^2)$  via the unitary matrix

$$U_{\tilde{t}} = \begin{pmatrix} \cos \theta_{\tilde{t}} & \sin \theta_{\tilde{t}} e^{i\gamma_t} \\ -\sin \theta_{\tilde{t}} e^{-i\gamma_t} & \cos \theta_{\tilde{t}} \end{pmatrix} \quad (3)$$

whose entries have the meaning

$$\begin{aligned}
\tan 2\theta_{\tilde{t}} &= -\frac{2m_t\tilde{A}_t}{m_L^2 - m_R^2} \\
\tan \gamma_t &= \frac{|A_t|\sin\gamma_A + |\mu|\cot\beta\sin\gamma_\mu}{|A_t|\cos\gamma_A - |\mu|\cot\beta\cos\gamma_\mu} \\
\tilde{A}_t &= [|A_t|^2 + |\mu|^2\cot^2\beta - 2|A_t||\mu|\cot\beta\cos(\gamma_\mu + \gamma_A)]^{1/2}
\end{aligned} \tag{4}$$

where  $\gamma_A \equiv \text{Arg}\{A_f\}$ ,  $\gamma_\mu \equiv \text{Arg}\{\mu\}$ . The mass eigenstate stops are denoted by  $\tilde{t}_1$  and  $\tilde{t}_2$ , with  $m_{\tilde{t}_1} < m_{\tilde{t}_2}$ , where

$$m_{\tilde{t}_1(\tilde{t}_2)} = (1/2)(2m_t^2 + M_L^2 + M_R^2 - (+)\sqrt{(M_L^2 - M_R^2)^2 + 4m_t^2\tilde{A}_t^2}). \tag{5}$$

Since  $\tilde{A}_t$  increases as  $\gamma_A + \gamma_\mu$  increases from zero to  $\pi$ ,  $m_{\tilde{t}_1}$  ( $m_{\tilde{t}_2}$ ) decreases (increases) with  $\gamma_A + \gamma_\mu$ . Therefore,  $m_{\tilde{t}_1}$  becomes minimal for CP phases around  $\pi$ . This point will be useful in discussing the radiative corrections to scalar–pseudoscalar– $Z$  boson vertex.

For computing the radiative corrections to Higgs masses and mixings one applies the usual procedure, that is, the stop mass-squared matrix (2) is diagonalized to obtain field dependent stop masses which are inserted to the effective potential formulae (1) together with the field dependent mass for the top quark. Then the second order derivatives of (1) evaluated at the stationarity point give the radiatively-corrected Higgs mass-squared matrix. One can find detailed expressions for the elements of Higgs mass-squared matrix in [11] which uses the basis  $\mathcal{B} = (\mathcal{R}e[H_1^0], \mathcal{R}e[H_2^0], A \equiv \sin\beta\mathcal{I}m[H_1^0] + \cos\beta\mathcal{I}m[H_2^0])$ . Diagonalization of the Higgs mass-squared matrix produces three mass-eigenstate scalars  $H_1, H_2, H_3$  which are chosen to correspond to  $h, H$  and  $A$  at  $\gamma_A = 0$ , respectively. Symbolically one has

$$\begin{pmatrix} H_1 \\ H_2 \\ H_3 \end{pmatrix} = \begin{pmatrix} R_{11} & R_{12} & R_{13} \\ R_{21} & R_{22} & R_{23} \\ R_{31} & R_{32} & R_{33} \end{pmatrix} \begin{pmatrix} \mathcal{R}e[H_1^0] \\ \mathcal{R}e[H_2^0] \\ A \end{pmatrix}. \tag{6}$$

From this matrix equality it is obvious that the mass-eigenstate scalars  $H_i$  are no longer CP eigenstates. This CP-breaking follows from the associated entries of the Higgs mass-squared matrix which are all proportional to  $\sin(\gamma_A + \gamma_\mu)$ ; namely, CP-violation in the Higgs sector is lifted once the supersymmetric CP-phases vanish [11]. Elements of the matrix  $R$  characterize the CP-violation in the Higgs sector and they appear in couplings of  $H_i$  to fermions, gauge bosons, and other Higgs particles as well [11,13]. To compute the radiative corrections to scalar–pseudoscalar– $Z$  boson vertex in the presence of the supersymmetric CP-phases one needs Feynman rules for certain vertices. The  $Z$  boson couples to Higgs particles and stops as follows:

$$\begin{aligned}
V_{ZH_iH_j} &= (\cos\beta R_{j2} - \sin\beta R_{j1})R_{i3} - (\cos\beta R_{i2} - \sin\beta R_{i1})R_{j3} \\
V_{Z\tilde{t}_1\tilde{t}_1} &= -i\left(\frac{1}{2}\cos^2\theta_{\tilde{t}} - \frac{2}{3}s_W^2\right) \\
V_{Z\tilde{t}_1\tilde{t}_2} &= -i\frac{1}{4}\sin 2\theta_{\tilde{t}}e^{i\gamma_t} \\
V_{Z\tilde{t}_2\tilde{t}_1} &= -i\frac{1}{4}\sin 2\theta_{\tilde{t}}e^{-i\gamma_t} \\
V_{Z\tilde{t}_2\tilde{t}_2} &= -i\left(\frac{1}{2}\sin^2\theta_{\tilde{t}} - \frac{2}{3}s_W^2\right)
\end{aligned} \tag{7}$$

where  $i, j = 1, 2, 3$ . For future convenience,  $V_{Z\tilde{t}_1\tilde{t}_1}$  is given in units of  $G \equiv \sqrt{g^2 + g'^2}$ , and  $V_{ZH_iH_j}$  in units of  $G/2$  with their Lorentz structures suppressed. On the other hand, the CP-odd componenet of  $H_i$  couples to stops as follows

$$\begin{aligned} V_{H_i\tilde{t}_1\tilde{t}_1}^{(P)} &= \frac{1}{2} \sin 2\theta_{\tilde{t}}(A_P^i - A_P^{i*}) \\ V_{H_i\tilde{t}_2\tilde{t}_2}^{(P)} &= -\frac{1}{2} \sin 2\theta_{\tilde{t}}(A_P^i - A_P^{i*}) \\ V_{H_i\tilde{t}_1\tilde{t}_2}^{(P)} &= \sin^2 \theta_{\tilde{t}} A_P^i e^{i\gamma_t} + \cos^2 \theta_{\tilde{t}} A_P^{i*} e^{-i\gamma_t} \\ V_{H_i\tilde{t}_2\tilde{t}_1}^{(P)} &= -(\cos^2 \theta_{\tilde{t}} A_P^i e^{-i\gamma_t} + \sin^2 \theta_{\tilde{t}} A_P^{i*} e^{-i\gamma_t}) \end{aligned} \quad (8)$$

where  $A_P^i = (|A_t| \cos \beta e^{i\gamma_A} + |\mu| \sin \beta e^{-i\gamma_\mu}) e^{i\gamma_t} R_{i3}$  shows the effects of the stop left-right mixings on the couplings of the CP-odd component of  $H_i$ . Finally, the CP-even component of  $H_i$  couples to stops via

$$\begin{aligned} V_{H_i\tilde{t}_1\tilde{t}_1}^{(S)} &= i\left\{\frac{4}{3}\frac{M_Z^2}{m_t}s_W^2\left(1 + \frac{3-8s_W^2}{4s_W^2}\cos^2\theta_{\tilde{t}}\right)\sin\beta(\cos\beta R_{i1} - \sin\beta R_{i2}) + 2m_t R_{i2}\right. \\ &\quad \left.- \frac{1}{2}\sin 2\theta_{\tilde{t}}(A_S^i + A_S^{i*})\right\} \\ V_{H_i\tilde{t}_2\tilde{t}_2}^{(S)} &= i\left\{\frac{4}{3}\frac{M_Z^2}{m_t}s_W^2\left(1 + \frac{3-8s_W^2}{4s_W^2}\sin^2\theta_{\tilde{t}}\right)\sin\beta(\cos\beta R_{i1} - \sin\beta R_{i2}) + 2m_t R_{i2}\right. \\ &\quad \left.+ \frac{1}{2}\sin 2\theta_{\tilde{t}}(A_S^i + A_S^{i*})\right\} \\ V_{H_i\tilde{t}_1\tilde{t}_2}^{(S)} &= i\left\{\frac{1}{6}\frac{M_Z^2}{m_t}(3-8s_W^2)\sin 2\theta_{\tilde{t}}\sin\beta(\cos\beta R_{i1} - \sin\beta R_{i2})e^{\gamma_t}\right. \\ &\quad \left.+ \cos^2\theta_{\tilde{t}}A_S^{i*}e^{i\gamma_t} - \sin^2\theta_{\tilde{t}}A_S^ie^{i\gamma_t}\right\} \\ V_{H_i\tilde{t}_2\tilde{t}_1}^{(S)} &= i\left\{\frac{1}{6}\frac{M_Z^2}{m_t}(3-8s_W^2)\sin 2\theta_{\tilde{t}}\sin\beta(\cos\beta R_{i1} - \sin\beta R_{i2})e^{-\gamma_t}\right. \\ &\quad \left.+ \cos^2\theta_{\tilde{t}}A_S^ie^{-i\gamma_t} - \sin^2\theta_{\tilde{t}}A_S^{i*}e^{-i\gamma_t}\right\} \end{aligned} \quad (9)$$

where  $A_S^i = (|A_t|R_{i2}e^{i\gamma_A} - |\mu|R_{i1}e^{-i\gamma_\mu})e^{i\gamma_t}$  summarizes nothing but the effects of stop left-right mixings on the CP-even component of  $H_i$ . All  $H_i$  to  $\tilde{t}_a\tilde{t}_b$  couplings listed in (8) and (9) are given in units of  $h_t/\sqrt{2}$  for future convenience.

Couplings of the Higgs scalars to stops depend on several parameters coming from the mass-squared matrices of stops and Higgs scalars. Among all, stop left-right mixing angle  $\theta_{\tilde{t}}$ , CP-breaking phases  $\gamma_{A,t}$  and Higgs mixing parameters  $R_{ij}$  are particularly interesting. The CP-violating supersymmetric phases enter all couplings in (7)-(9), masses of the Higgs scalars and stops, and Higgs mixing matrix  $R$ . These phases not only modify the couplings existing in the CP-invariant theory, but also create new ones as the expressions of  $V_{H_i\tilde{t}_1\tilde{t}_1}^{(P)}$  and  $V_{H_i\tilde{t}_2\tilde{t}_2}^{(P)}$  show explicitly. These two couplings are created solely by the supersymmetric CP phases and necessarily vanish in the CP-conserving limit:  $\gamma_{A,\mu} \rightarrow 0$ .

When the off-diagonal elements of the stop mass-squared matrix are large (provided the light stop mass in above the present LEP lower bound of  $\sim 75$  GeV) compared to its diagonal elements, the stop mixing becomes maximal, that is,  $\sin 2\theta_{\tilde{t}} \rightsquigarrow 1$ . In this limit,  $Z$  to  $\tilde{t}_a\tilde{t}_{b \neq a}$ ,

$H_i^P$  to  $\tilde{t}_a\tilde{t}_b$ , and  $H_i^S$  to  $\tilde{t}_a\tilde{t}_a$  couplings are maximized as seen from (7)-(9). Of course such statements depend on relative strengths of  $|A_t|$  and  $|\mu|$  as well as their phases. In essence, one needs large chiral mixings to highlight the effects of novel  $H_i^P\tilde{t}_a\tilde{t}_a$  couplings; however, in this limit  $H_i^S\tilde{t}_a\tilde{t}_a$  and  $H_i^P\tilde{t}_a\tilde{t}_{b\neq a}$  couplings (which exist in the CP-conserving limit too) become also large though the corresponding formfactors are expected to be suppressed partially by heavy  $\tilde{t}_2$ . The CP-compositions of the Higgs scalars are dictated by  $R_{ij}$ ; hence, whatever the strengths of the one-loop vertex corrections, they constitute the envelope of the effective scalar-pseudoscalar- $Z$  boson vertices. These points will be clearer when the explicit numerical computation is carried out.

For a proper analysis of the Higgs pair production, it is not sufficient to compute the radiative corrections to Higgs masses and couplings, one has to compute also the radiative corrections to scalar-pseudoscalar- $Z$  boson vertex. Once the radiative corrections are switched on vector boson self energies as well as the vertex formfactors need be computed with the inclusion of the entire MSSM particle spectrum [6]. However, consistent with the description of the Higgs sector, dominant corrections come from the top quark and top squark loops. Using the form of the radiatively-corrected cross section [6] one can easily incorporate the radiative corrections to ‘tree’ vertex  $V_{ZH_iH_j}$  as follows

$$\begin{aligned}\hat{V}_{ZH_iH_j} = & V_{ZH_iH_j} + \beta_{h_t} \{ \cos \beta (R_{i2}R_{j3} - R_{j2}R_{i3}) \mathcal{Q}_t(-p_i, p_j, m_t, m_t, m_t) \\ & + (V_{Z\tilde{t}_b\tilde{t}_c} V_{H_i\tilde{t}_a\tilde{t}_b}^{(S)} V_{H_j\tilde{t}_c\tilde{t}_a}^{(P)} - V_{Z\tilde{t}_c\tilde{t}_b} V_{H_i\tilde{t}_b\tilde{t}_a}^{(P)} V_{H_j\tilde{t}_a\tilde{t}_c}^{(S)}) \mathcal{Q}_{\tilde{t}}(-p_i, p_j, m_{\tilde{t}_a}, m_{\tilde{t}_b}, m_{\tilde{t}_c}) \} \end{aligned} \quad (10)$$

where  $\beta_{h_t} = 3h_t^2/(16\pi^2)$ , summation of  $a, b = 1, 2$  is implied, and top quark and top squark triangles are represented by the loop functions  $\mathcal{Q}_t(-p_i, p_j, m_t, m_t, m_t)$  and  $\mathcal{Q}_{\tilde{t}}(-p_i, p_j, m_{\tilde{t}_a}, m_{\tilde{t}_b}, m_{\tilde{t}_c})$ , respectively. These vertex formfactors could be expressed in terms of the standard Veltman-Passarino loop functions [19] as follows

$$\begin{aligned}\mathcal{Q}_t(p, q, m, m, m) = & B_0(p - q, m) + 2m^2 C_0(p, q, m, m, m) + p^2 C_1(p, q, m, m, m) \\ & + q^2 C_2(p, q, m, m, m) \\ \mathcal{Q}_{\tilde{t}}(p, q, m_a, m_b, m_c) = & -2(C_0(p, q, m_a, m_b, m_c) + C_1(p, q, m_a, m_b, m_c) \\ & + C_2(p, q, m_a, m_b, m_c)) \end{aligned} \quad (11)$$

where the notation and definitions of [20] are adopted. Here  $p_i^2 = M_{H_i}^2$ ,  $p_j^2 = M_{H_j}^2$  and  $2p_i \cdot p_j = s - M_{H_i}^2 - M_{H_j}^2$ . The light stop contribution is finite whereas the top quark contribution, due to  $B_0$  function, has a UV divergence,  $\Delta$ , which is renormalized with minimal prescription as was done for the effective potential (1). Moreover,  $B_0$  has a scale dependence through  $\log m_t^2/Q^2$ .

There are several aspects of (10) deserving a detailed discussion. First, one notes that top quark contribution is proportional to  $\cos \beta$ , which means that this contribution is suppressed for large  $\tan \beta$  (before bottom and tau Yukawa couplings become comparable to top Yukawa coupling). In the same way  $V_{ZH_iH_j}$  gets diminished for large  $\tan \beta$  [7,18] especially when  $|R_{i3}|$  is negligably small (this will be seen to hold in  $H_1 H_{j\neq 1}$  production). Unlike  $V_{ZH_iH_j}$  and top quark loop contribution, however, the stop contribution is not necessarily suppressed in the large  $\tan \beta$  regime due to the fact that it has both  $\sin \beta$  and  $\cos \beta$  dependencies weighted by  $|A_t|$  and  $|\mu|$  as seen from the expression of  $A_P^i$  below (8). In this way one expects

stop contributions to lead important variations in the effective vertex depending on the supersymmetric parameter space adopted. From eq. (8) one observes that the coupling of  $H_i^P$  to  $\tilde{t}_1\tilde{t}_1$  pair is purely imaginary so that its contribution to  $|\hat{V}_{ZH_iH_j}|$  remains at the two-loop order unless  $\mathcal{Q}_{\tilde{t}}(-p_i, p_j, m_{\tilde{t}_1}, m_{\tilde{t}_1}, m_{\tilde{t}_1})$  develops an absorptive part part entailing an interference with  $V_{ZH_iH_j}$  and the dispersive part of the top quark contribution. These observations require light stop be light enough (weighing  $\sim m_t$ ) to have stop contributions be enhanced.

To have better understanding of the role of the supersymmetric phases on Higgs pair production it is convenient to analyze the one-loop vertex (10) numerically. However, for this purpose it is necessary to have a detailed knowledge of the mixing matrix  $R$  to identify the CP-impurities of the Higgs bosons. In the numerical analysis below we shall adopt the following parameter values

$$M_{\tilde{L}} = M_{\tilde{R}} = 500 \text{ GeV}; |A_t| = 1.3 \text{ TeV}; |\mu| = \mu = 250 \text{ GeV}; \tilde{M}_A = 200 \text{ GeV} \quad (12)$$

having in mind an  $e^+e^-$  collider with  $\sqrt{s} = 500 \text{ GeV}$  (for example the recently planned TESLA facility [17]). Here  $\tilde{M}_A$  is analogous to pseudoscalar mass  $M_A$  in the CP-invariant theory [15], and its definition can be found in [11]. In the analysis, phase of  $A_t$ ,  $\gamma_A$ , is treated as a free variable whereas  $\gamma_\mu$  is set to zero. In each case  $\tan\beta = 2$  and  $30$  are considered separately to illustrate low and high  $\tan\beta$  cases, respectively. Depicted in Figures 1-3 are the  $\gamma_A$  dependence of the percentage compositions of  $H_1$ ,  $H_2$  and  $H_3$ . Fig. 1 shows  $R_{11}^2$  (solid curve),  $R_{12}^2$  (dashed curve), and  $R_{13}^2$  (dotted curve) for  $\tan\beta = 2$  (left panel) and  $\tan\beta = 30$  (right panel). As the figure suggests,  $\tan\beta = 2$ , CP-even components of  $H_1$  oscillate between  $\sim 45\%$  and  $\sim 55\%$  in the entire  $\gamma_A$  range while its CP-odd component remains below  $1\%$  everywhere. The right panel shows the  $\gamma_A$  dependence of the same quantities for  $\tan\beta = 30$ , from which it is seen that  $R_{12}^2$  remains above  $\sim 90\%$ , and correspondingly  $R_{11}^2$  is always below  $\sim 10\%$  line. This rearrangement of the CP-even components results from the large value of  $\tan\beta$  as in the CP-invariant theory [7]. Similar to Fig. 1 the CP-odd composition of  $H_1$  is rather small, never exceeding  $\sim 0.5\%$  level. That the lightest Higgs ( $H_1$ ) remains essentially CP-even follows from the decoupling between the heavy and light sectors in the MSSM Higgs sector [12,11,13]. Indeed, if  $\tilde{M}_A$  were lighter (say below  $\sim 150 \text{ GeV}$  with a low enough  $\tan\beta$ )  $H_1$  would have a larger CP=-1 composition.

Fig. 2 shows  $\gamma_A$  dependence of  $R_{21}^2$  (solid curve),  $R_{22}^2$  (dashed curve), and  $R_{23}^2$  (dotted curve) for  $\tan\beta = 2$  (left panel) and  $\tan\beta = 30$  (right panel). As is seen from Fig. 3, for  $\gamma_A \rightarrow 0$ ,  $H_2$  becomes the usual heavy CP-even Higgs boson of the MSSM, its CP-even components start at  $\gamma_A = 0$  in agreement with Fig. 1 (left panel), and completely vanish at  $\gamma_A = \pi$  at which it becomes a completely CP-odd Higgs boson. Indeed,  $H_2$  assumes a definite CP property for  $\sin\gamma_A \rightarrow 0$ ; however, it has opposite CP quantum numbers for  $\gamma_A = 0$  and  $\gamma_A = \pi$ . Switching to Fig. 2 right panel one observes an even stronger CP-impurity for  $H_2$ : Except for  $\gamma_A \lesssim 1$  (and of course  $\gamma_A \gtrsim 5$ )  $H_2$  is almost a pure CP-odd Higgs boson where its CP-even composition remains below  $\sim 12\%$ . As in Fig. 3 for  $\gamma = \pi$   $H_2$  is purely CP-odd. The strong CP-impurity of  $H_2$  automatically implies a symmetric situation for  $H_3$  (the would-be CP-odd boson of the CP-invariant theory) as suggested by Fig. 3. Indeed  $H_2$  and  $H_3$  are complementary to each other in the sense that  $H_3$  is mostly CP-even in regions where  $H_2$  is nearly CP-odd. The lesson drawn from Figs. 1-3

is that the lightest Higgs  $H_1$  keeps becoming, to a good approximation, CP-even while the other two Higgs scalars mix with each other significantly depending on  $\gamma_A$  and  $\tan\beta$ . In forming these graphs use has been made of the parameter set in (8) in which  $\tilde{M}_A$  is fixed to 200 GeV. Similar to  $M_A$  of the CP-invariant theory  $\tilde{M}_A$  determines the masses of heavy scalars  $H_2$  and  $H_3$ . Together with large  $\tan\beta$  values, large  $\tilde{M}_A$  values imply the decoupling limit described in [7]. However, for collider applications (with  $\sqrt{s} = 500$  GeV as considered here) it is necessary to keep  $\tilde{M}_A$  around 200 GeV to allow for pair production of the Higgs scalars. In accordance with the results of [11], on the average,  $M_{H_1} = 130$  GeV (155 GeV),  $M_{H_2} = 210$  GeV (200 GeV), and  $M_{H_3} = 200$  GeV (200 GeV) for  $\tan\beta = 2(30)$  in the entire range of  $\gamma_A$ . Therefore, with  $\sqrt{s} = 500$  GeV, it is possible to produce even  $H_2 - H_3$  pairs despite strong kinematic suppression compared to  $H_1 - H_2$  or  $H_1 - H_3$  productions.

The CP compositions of  $H_2$  and  $H_3$  shown in Figs. 2 and 3 need further discussion. One notices that  $\gamma_A = 0$  and  $\gamma_A = \pi$  are equivalent in the sense that CP-breaking components of the Higgs mass-squared matrix vanish at both points. However, according to the CP compositions of  $H_2$  and  $H_3$  these points are no longer equivalent. This follows from the fact that the radiative corrections at these two points are no longer equivalent since the quantities involving  $\cos\gamma_{A,\mu}$  (which remain non-vanishing in the CP-conserving limit) reverse their sign as one switches from  $\gamma_A = 0$  to  $\gamma_A = \pi$ . Therefore, as an example, one observes from (5) that for  $\gamma_A = \pi$  light stop (heavy stop) assumes its smallest (largest) possible mass for a given parameter space. This then maximizes  $\log m_{\tilde{t}_2}^2/m_{\tilde{t}_1}^2$  type stop-splitting contributions modifying the strength of the radiative corrections. Other than all these, diagonalization of the Higgs mass-squared matrix (described in (6)) uses only the properties of the scalars at  $\gamma_A = 0$  in naming them, and does not care their behaviour at finite  $\gamma_A$ .

Given the CP-properties of the Higgs bosons in Figs. 1-3, and the effective scalar-pseudoscalar- $Z$  boson vertex in (10) then one can analyze the effective vertex  $|\hat{V}_{ZH_iH_j}|$  by identifying the loop and tree-level contributions for each  $H_i$ . For the parameter set in (12), the light stop mass start with 274 GeV (234 GeV) at  $\gamma_A = 0$ , and falls to 177 GeV (227 GeV) at  $\gamma_A = \pi$  for  $\tan\beta = 2$  (30). For  $\tan\beta = 2$ ,  $m_{\tilde{t}_1}$  falls below 250 GeV at  $\gamma_A \sim 1$ .

Depicted in Fig. 4 is the  $\gamma_A$  dependence of  $|\hat{V}_{ZH_1H_3}|$  for  $\tan\beta = 2$  (left panel) and  $\tan\beta = 30$  (right panel). Here solid curve shows  $|V_{ZH_1H_3}|$  which includes no vertex corrections. For  $\tan\beta = 2$  (left panel)  $|V_{ZH_1H_3}| \sim 0.36$  at  $\gamma_A = 0$ , and it gradually decreases with increasing  $\gamma_A$  eventually vanishing at  $\gamma_A = \pi$ . This behaviour is dictated by the left panels of Figs. 1 and 3 where  $H_1$  remains essentially CP-even for all  $\gamma_A$  whereas  $H_3$  becomes a pure CP-even scalar in a narrow region around  $\gamma_A = \pi$ . The dashed curve shows  $|\hat{V}_{ZH_1H_3}|$  when only the top quark loop is considered. The top quark loop is seen to contribute by  $\sim 0.5\%$  and has essentially the same  $\gamma_A$  dependence as the solid curve. This essentially follows from the dominance of the ‘tree-vertex’  $V_{ZH_1H_3}$ . Here one notes that the absorptive part of the top quark loop does not interfere with  $V_{ZH_1H_3}$  and becomes a two-loop effect in computing  $|\hat{V}_{ZH_1H_3}|$ . When the scalar top quark loops (dotted curve) are included, however, one gets a  $\sim 6\%$  enhancement in  $|V_{ZH_1H_3}|$  at  $\gamma = 0$ . This amount of enhancement is typical of this process as already noted in [6]. This large correction is due to the fact that  $H_i^{S,P}$  to  $\tilde{t}_1\tilde{t}_2$  couplings are large because of relatively large value of  $|A_t|$ . In fact, in the CP-conserving limit  $H_i^P$  couples only distinct stops so that the stop loop involves at least one  $\tilde{t}_2$ .  $|\hat{V}_{ZH_1H_3}|$  starts with this relatively large value at  $\gamma_A = 0$ , and decreases faster than the previous two



until  $\gamma_A \sim 1.1$ . This decrease follows from the gradual increase in  $m_{\tilde{t}_2}$  suppressing the vertex formfactors. In this region  $\gamma_A$  dependence are dictated by  $R_{ij}$  and the vertices listed in (7)-(9). At  $\gamma_A \sim 1.1$ , however, it changes sharply due to the fact that  $\mathcal{Q}_{\tilde{t}}(-p_i, p_j, m_{\tilde{t}_1}, m_{\tilde{t}_1}, m_{\tilde{t}_1})$  now develops an absorbtive part (since at  $\gamma_A \sim 1.1$   $m_{\tilde{t}_1}$  just falls below  $\sqrt{s}/2$ ) which, when multiplied by the purely imaginary vertex  $V_{H_3\tilde{t}_1\tilde{t}_1}^{(P)}$ , becomes pure real and interferes with the ‘tree-level’ vertex  $V_{ZH_1H_3}$  modifying it sharply. It is this kind of behaviour that shows clearly the effects of the pure light stop loop existing solely due to the CP-violation. Asymmetric behaviour of  $|\hat{V}_{ZH_1H_3}|$  with respect to  $\gamma_A = \pi$  axis as well as its coincidences with  $|V_{ZH_1H_3}|$  follows from the  $\gamma_A$  dependence of vertices listed in (7)-(9): It behaves as  $\sim \sin 2\gamma \cos 2\gamma$  appropriate for  $\gamma_\mu = 0$  and  $|A_t| \gg |\mu|$ .

The right panel of Fig. 4 shows the  $\gamma_A$  dependence of  $|\hat{V}_{ZH_1H_3}|$  for  $\tan\beta = 30$ . One observes first decrease in the strength of all curves compared to the left panel. One observes several differences between this figure and the left panel: First, as mentioned before, the light stop mass is below the  $\sqrt{s}/2$  for the entire range of  $\gamma$  so that there is no sharp change in the variation of the figure at any value of  $\gamma_A$ . Second, the comparatively fast variation of  $|\hat{V}_{ZH_1H_3}|$  follows the right panels of Figs. 1 and 3 where  $\phi_2$  component of  $H_1$  remains large whereas the CP-odd component of  $H_3$  is diminished rather fast (see the dotted curve in Fig. 3, right panel). It is for this reason that  $|\hat{V}_{ZH_1H_3}|$  oscillates faster than in left panel. Third,  $|\hat{V}_{ZH_1H_3}|$  for  $\tan\beta$  is rescaled to smaller values compared to the left panel. This follows from the large value of  $\tan\beta$  which is known to suppress tree as well as the one-loop corrections [6]. However, the gain in  $|\hat{V}_{ZH_1H_3}|$  with respect to its value at  $\gamma_A = 0$  is much larger than the one in the left panel. For example, around  $\gamma_A \sim 2.5$   $|\hat{V}_{ZH_1H_3}|$  is  $\sim 2.3$  times bigger than its value at  $\gamma_A = 0$ . Finally one notices that, at large  $\tan\beta$ , almost entire behaviour of  $|\hat{V}_{ZH_1H_3}|$  is determined by the ‘tree-vertex’  $V_{ZH_1H_3}$ ; the one-loop corrections are suppressed compared to the left panel. In this limit top quark contribution is suppressed by  $\cos\beta$  factor it multiplies, on the other hand, stop contributions are suppressed by the  $\cos\beta$  factor multiplying  $|A|_t$  ( $|\mu|$  is already small) in  $A_P^i$  and by similar factors in  $A_S^i$ .

As is seen from Fig. 2  $H_2$  (which becomes  $H$  at  $\gamma_A = 0$ ) is no longer a CP-even Higgs as  $\gamma_A$  varies. Thus, it is possible to produce  $H_1H_2$  pairs in addition to  $H_1H_3$  detailed above. As expected,  $|\hat{V}_{ZH_1H_2}|$  vanishes at  $\gamma_A = 0$  at which both scalars are CP-even. In similarity with the discussions concerning  $|\hat{V}_{ZH_1H_3}|$  above one can analyze this process too. For example, minima and maxima of the effective vertex follow from their CP compositions in Figs. 2 and 3 using repetitive panels. In general since the vertex is generated by the CP-violation in the Higgs sector, rather than the vertex radiative corrections, behaviour of  $|\hat{V}_{ZH_1H_2}|$  is mainly dictated by  $V_{ZH_1H_2}$  everywhere. One finally notices that the effects of the absorbtive part of the light stop contribution is too small to be seen in the variation of  $V_{ZH_1H_2}$ .

In principle one can also analyze the effective vertex for  $H_2H_3$  production. However, for the collider search the main concern is the associated production of  $H_1$  with a heavy Higgs scalar as this is the first step towards a complete discovery of the Higgs spectrum of the MSSM. Moreover, for the center-of-mass energy chosen in this work pair production of such heavy scalars will be suppressed. In spite of these facts, however, from the comparison of Figs. 2-3 it is obvious that  $|\hat{V}_{ZH_2H_3}|$  will not have a significant  $\gamma_A$  dependence because these two scalars have complementary CP-properties. One expects similar effects to occur in other Higgs boson couplings [11].

### III. DISCUSSIONS AND CONCLUSION

This work has concentrated on the associated production of one light and one heavy Higgs scalars in the presence of explicit CP violation due to non-vanishing supersymmetric CP phases. In the light of the results derived in the text one can state that: (i) The lightest of the three Higgs scalars remains essentially CP-even due to decoupling between the light and heavy sectors in the MSSM [7], and this is also confirmed by [11,13]. (ii) Due to this CP-purity of the lightest Higgs  $e^+e^- \rightarrow H_i H_j$  probe only the CP-odd composition of the heavy scalar; therefore, assuming sufficient mass resolution at next generation of colliders one expects MSSM to behave as having two CP-odd Higgs bosons for certain values of the supersymmetric CP-phases. (iii) Explicit CP-violation not only mixes scalars of different CP-properties but also induces a novel vertex where a CP-odd Higgs boson can couple to identical sfermions. Effects of this additional interaction rule has been shown to be observable by through the phase dependence of the one-loop scalar-pseudoscalar- $Z$  boson vertex. However, this additional interaction can show up most significantly in the *pseudoscalar*  $\rightarrow \gamma\gamma$  decay whose rate gets no contribution from the sfermion loops in the absence of CP-violation. (iv) The explicit CP-violation discussed here, in particular the relations among vertices coupling Higgs scalars to gauge bosons and fermions, are special cases of the general rules described in [22].

This work as well as others [12,11,13] assume the existence of non-vanishing phases for  $\mu$  parameter and all other soft mass parameters. Though it is not essential for low-energy supersymmetry phenomenology one can relate these phases to the Goldstone bosons of some broken global symmetries of the hidden sector in supergravity breaking [23]. As the analysis of [3] shows these phases generally relax to (near) a CP-conserving point in the case of universality. However, in more general cases, especially when the supersymmetry breaking in the hidden sector is realized non-linearly, these phases may relax to some point away from the CP-conserving limit. In this sense, it is this possibility that is investigated here. As the graphs of the effective vertices in Figs. 4-5 show, if these phases relax to points away from the CP-conserving point they can have drastic implications for the collider phenomenology of Higgs bosons [12,11,13], and also for Kaon and B-meson phenomenology [14]. Finally one notes the acceleration in the interest to the supersymmetric CP-phases in the context of the electroweak baryogenesis [24].

### IV. ACKNOWLEDGEMENTS

The author is grateful to A. Masiero, A. Pilaftsis, J. Rosiek, G. Senjanovic and C. E. M. Wagner for stimulating discussions about various aspects of this work. He also thanks to CERN Theory Division where this work is completed.

## REFERENCES

- [1] J. Rosiek, *Phys. Rev.* **D41** (1990) 3464; (E) hep-ph/9511250.
- [2] M. Dugan, B. Grinstein and L. J. Hall, *Nucl. Phys.* **B255** (1985) 413.
- [3] S. Dimopoulos and S. Thomas, *Nucl. Phys.* **B465** (1996) 23.
- [4] NLC ZDR Design Group, NLC Physics Working Group, hep-ex/9605011.
- [5] J. F. Gunion and H. E. Haber, hep-ph/9806330.
- [6] P. H. Chankowski, S. Pokorski, J. Rosiek, *Nucl. Phys.* **B423** (1994) 437; 497.
- [7] H. E. Haber, hep-ph/9505240.
- [8] T. Falk, K. A. Olive, *Phys. Lett.* **B375** (1996) 196.
- [9] T. Falk, K. A. Olive, M. Srednicki, *Phys. Lett.* **B354** (1995) 99.
- [10] J. Ellis, S. Ferrara and D. V. Nanopoulos *Phys. Lett.* **B114** (1982) 231; W. Buchmüller and D. Wyler, *Phys. Lett.* **B121** (1983) 321; J. Polchinski and M. Wise, *Phys. Lett.* **B125** (1983) 393; F. del Aguila, M. Gavela, J. Grifols and A. Mendez, *Phys. Lett.* **B126** (1983) 71; D. V. Nanopoulos and M. Srednicki, *Phys. Lett.* **B128** (1983) 61; Y. Kizukuri and N. Oshimo, *Phys. Rev.* **D46** (1992) 3025; S. A. Abel and J. M. Frere *Phys. Rev.* **D55** (1997) 1623; T. Ibrahim and P. Nath, *Phys. Rev.* **D57** (1998) 478; *Phys. Rev.* **D58** (1998) 111301; M. Brhlik, G. J. Good and G. L. Kane, hep-ph/9810457.
- [11] D. A. Demir, hep-ph/9901389 (to appear in *Phys. Rev. D*).
- [12] A. Pilaftsis, *Phys. Rev.* **D58** (1998) 096010; *Phys. Lett.* **B435** (1998) 88.
- [13] A. Pilaftsis and C. E. M. Wagner, hep-ph/9902371 (to appear in *Nucl. Phys. B*).
- [14] D. A. Demir, A. Masiero and O. Vives, *Phys. Rev. Lett.* **82** (1999) 2447.
- [15] A. Brignole, *Phys. Lett.* **B277** (1992) 313; J. Ellis, G. Ridolfi, F. Zwirner, *Phys. Lett.* **B257** (1991) 83; **262** (1991) 477.
- [16] J. F. Gunion, A. Turski, *Phys. Rev.* **D39** (1989) 2701.
- [17] R. Brinkman, TESLA Collaboration, DESY-M-97-04, (1997); *Turk. J. Phys.* **22** (1998) 661.
- [18] J. F. Gunion, H. E. Haber, G. Kane, S. Dawson, "The Higgs Hunter's Guide", Addison-Wesley, New York, (1990).
- [19] G. 't Hooft, M. Veltman, *Nucl. Phys.* **B153** (1979) 365; G. Passarino, M. Veltman, *Nucl. Phys.* **B160** (1979) 151.
- [20] A. Denner, *Fortsch. Phys.* **41** (1993) 307.
- [21] T. J. Weiler, T.-C. Yuan, *Nucl. Phys.* **B318** (1989) 337.
- [22] B. Grzadkowski, J. F. Gunion, J. Kalinowski, hep-ph/9902308; J. F. Gunion, J. Pliszka, *Phys. Lett.* **B444** (1998) 136; L. Lavoura, J. P. Silva, *Phys. Rev.* **D48** (1993) 2356; A. Mendez, A. Pomarol, *Phys. Lett.* **B272** (1991) 313.
- [23] T. Banks, D. Kaplan, A. Nelson, *Phys. Rev.* **D49** (1994) 779; J. Bagger, E. Poppitz, L. Randall, *Nucl. Phys.* **B426** (1994) 3.
- [24] M. Carena, M. Quiros, A. Riotto, I. Vilja, C.E.M. Wagner, *Nucl. Phys.* **B503** (1994) 387; M. Carena, C.E.M. Wagner, hep-ph/9704347; K. Funakubo, S. Otsuki, F. Toyoda, hep-ph/9903276; J. Cline, M. Joyce, K. Kainulainen, *Phys. Lett.* **B417** (1998) 79; M. Laine, K. Rummukainen, hep-ph/9811369; K. Funakubo, hep-ph/9809517.

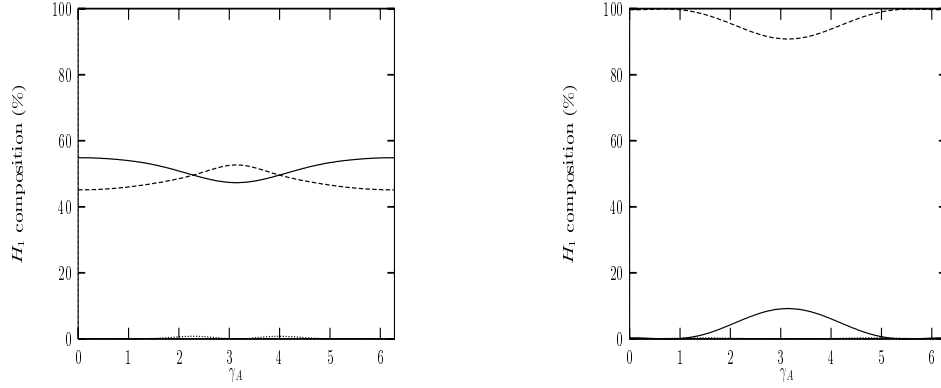


FIG. 1. Percentage composition of  $H_1$  as a function of  $\gamma_A$  for  $\tan \beta = 2$  (left panel) and  $\tan \beta = 30$  (right panel). Here  $R_{11}^2$ ,  $R_{12}^2$  and  $R_{13}^2$  are shown by solid, dashed, and dotted curves, respectively.

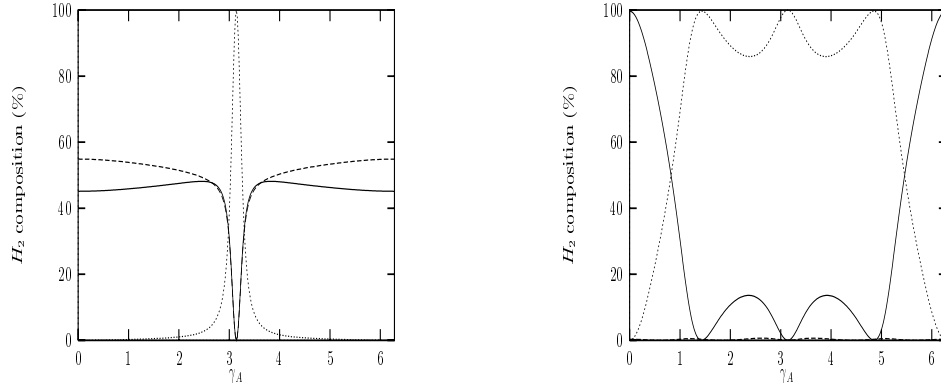


FIG. 2. Percentage composition of  $H_2$  as a function of  $\gamma_A$  for  $\tan \beta = 2$  (left panel) and  $\tan \beta = 30$  (right panel). Here  $R_{21}^2$ ,  $R_{22}^2$  and  $R_{23}^2$  are shown by solid, dashed, and dotted curves, respectively.

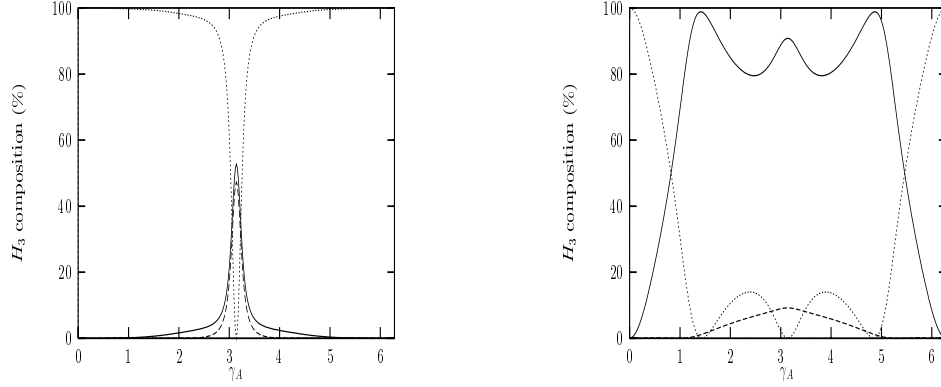


FIG. 3. Percentage composition of  $H_3$  as a function of  $\gamma_A$  for  $\tan \beta = 2$  (left panel) and  $\tan \beta = 30$  (right panel). Here  $R_{31}^2$ ,  $R_{32}^2$  and  $R_{33}^2$  are shown by solid, dashed, and dotted curves, respectively.

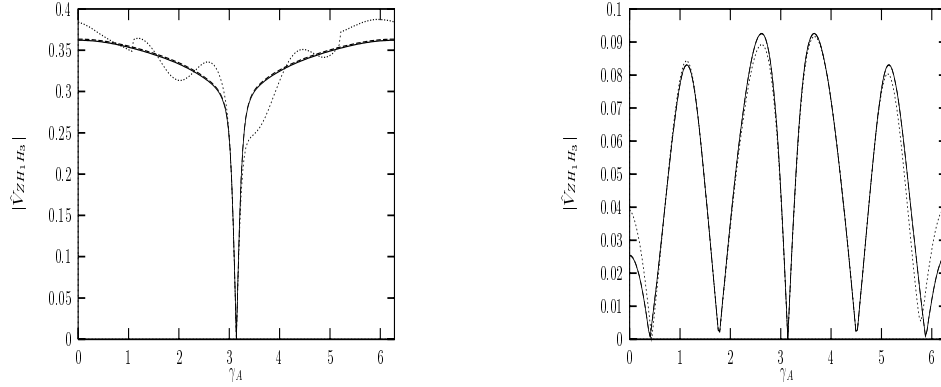


FIG. 4. Variation of  $\hat{V}_{ZH_1 H_3}$  with  $\gamma_A$  when there is no vertex corrections (solid curve), when only top quark contribution is included (dashed curve), and when both top quark and top squark loops are included (dotted curve). Here left panel stands for  $\tan \beta = 2$  and right panel for  $\tan \beta = 30$ .

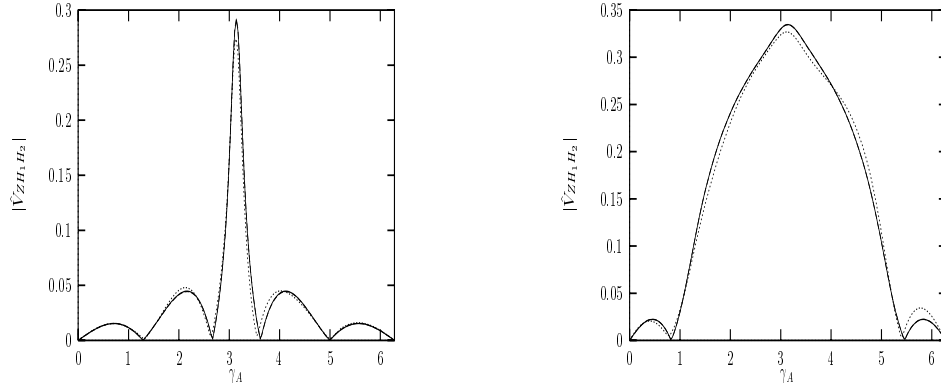


FIG. 5. Variation of  $\hat{V}_{ZH_1H_2}$  with  $\gamma_A$  when there is no vertex corrections (solid curve), when only top quark contribution is included (dashed curve), and when both top quark and top squark loops are included (dotted curve). Here left panel stands for  $\tan\beta = 2$  and right panel for  $\tan\beta = 30$ .